materials

MDPI

Article

Effect of Citric Acid Concentration on the Transformation of Aragonite $CaCO_3$ to Calcium Citrate Using Cockle Shells as a Green Calcium Source

Pantita Chanwetprasat [1], Chaowared Seangarun [1], Somkiat Seesanong [2], Banjong Boonchom [1,3,4,*], Nongnuch Laohavisuti [2,*], Wimonmat Boonmee [5] and Pesak Rungrojchaipon [4]

1 Material Science for Environmental Sustainability Research Unit, School of Science, King Mongkut's Institute of Technology Ladkrabang, Bangkok 10520, Thailand; 66056054@kmitl.ac.th (P.C.); chaowared@gmail.com (C.S.)
2 Office of Administrative Interdisciplinary Program on Agricultural Technology, School of Agricultural Technology, King Mongkut's Institute of Technology Ladkrabang, Bangkok 10520, Thailand; somkiat.se@kmitl.ac.th (S.S.)
3 Municipal Waste and Wastewater Management Learning Center, School of Science, King Mongkut's Institute of Technology Ladkrabang, Bangkok 10520, Thailand
4 Department of Chemistry, School of Science, King Mongkut's Institute of Technology Ladkrabang, Bangkok 10520, Thailand; pisak.ru@kmitl.ac.th
5 Department of Biology, School of Science, King Mongkut's Institute of Technology Ladkrabang, Bangkok 10520, Thailand; wimonmat.bo@kmitl.ac.th
* Correspondence: banjong.bo@kmitl.ac.th (B.B.); nongnuch.la@kmitl.ac.th (N.L.)

Abstract: Aragonite calcium carbonate ($CaCO_3$), derived from cockle shell waste, was successfully used as a renewable calcium source to synthesize calcium citrate (CCT) using citric acid ($C_6H_8O_7$). The three CCT products (CCT-2, CCT-3, and CCT-4) were prepared using three different acid concentrations: 2, 3, and 4 M. The physicochemical characteristics of the newly synthesized CCT were investigated. Fourier-transform infrared (FTIR) spectra revealed the vibrational modes of the citrate anionic group ($C_6H_5O_7^{3-}$), which preliminarily confirmed the characteristics of CCT. However, X-ray diffraction (XRD) revealed that the concentration of citric acid altered the structural property and the chemical formula of the synthesized CCT. Employing 2 M citric acid, a pure tetra-hydrated phase ($Ca_3(C_6H_5O_7)_2{\cdot}4H_2O$, earlandite mineral) was obtained. However, a mixture of hydrated ($Ca_3(C_6H_5O_7)_2{\cdot}4H_2O$) and anhydrous ($Ca_3(C_6H_5O_7)_2$) phases was precipitated when 3 and 4 M citric acid was used in the preparation process. The lower mass loss observed in the thermogravimetric analysis (TGA) of CCT-3 and CCT-4 compared to that of CCT-2 further confirmed that CCT-3 and CCT-4 were composed of hydrated and anhydrous CCTs. The synthesized CCT decomposed in four major processes: the first dehydration, the second dehydration, $CaCO_3$ formation, and decarbonization, generating calcium oxide (CaO) as the final product. X-ray fluorescence (XRF) results showed that the CCT mainly consisted of CaO with a quantity of >98%. The scanning electron microscopic (SEM) image revealed the irregular plate-like CCT crystallites. The concentration of citric acid is a key factor that influences the productive parameters of CCT, including production yield, reaction time, and solubility. 2 M citric acid provided the optimal balance between productivity and cost-effectiveness, with the highest yield and soluble fraction and the lowest reaction time. The results suggest that the preparation of CCT from cockle shell waste can potentially replace the use of commercial calcite from mining, which is a limited and non-renewable resource.

Keywords: calcium citrate; $Ca_3(C_6H_5O_7)_2{\cdot}4H_2O$; $CaCO_3$; cockle shell waste; citric acid; productivity

check for updates

Academic Editor: Nikolaos Bouropoulos

Received: 4 April 2025
Revised: 21 April 2025
Accepted: 25 April 2025
Published: 28 April 2025

Citation: Chanwetprasat, P.; Seangarun, C.; Seesanong, S.; Boonchom, B.; Laohavisuti, N.; Boonmee, W.; Rungrojchaipon, P. Effect of Citric Acid Concentration on the Transformation of Aragonite $CaCO_3$ to Calcium Citrate Using Cockle Shells as a Green Calcium Source. *Materials* **2025**, *18*, 2003. https://doi.org/10.3390/ma18092003

Copyright: © 2025 by the authors. Licensee MDPI, Basel, Switzerland. This article is an open access article distributed under the terms and conditions of the Creative Commons Attribution (CC BY) license (https://creativecommons.org/licenses/by/4.0/).

1. Introduction

Calcium citrate (CCT) is a critical organic calcium salt that can be applied in many industries, especially medicine [1] and food supplements [2]. CCT is often used as a calcium supplement because it is more bioavailable than calcium carbonate ($CaCO_3$) [3], one of the most common forms of calcium. CCT has been used in biomaterial fields such as rhBMP-2, which has shown a beneficial effect on osteoinduction and osteogenesis [4]. In nature, calcium citrate tetrahydrate ($Ca_3(C_6H_5O_7)_2{\cdot}4H_2O$) has been observed as an earlandite mineral in unconsolidated ocean floor sediment [5]. CCT compounds are typically synthesized through a chemical process using $CaCO_3$ [6], calcium chloride ($CaCl_2$) [7], or calcium nitrate tetrahydrate ($Ca(NO_3)_2{\cdot}4H_2O$) [8] as raw materials. It is also prepared by a microbial biomineralization process using fungi [9]. Among these raw materials, $CaCO_3$ is a common mineral form of calcium compound with the lowest value but the highest availability. $CaCO_3$ is widely used as a raw material for preparing value-added calcium materials, such as calcium lactate pentahydrate ($Ca(CH_3CHOHCOO)_2{\cdot}5H_2O$) [10].

$CaCO_3$ has three anhydrous crystalline polymorphs: hexagonal vaterite, orthorhombic aragonite, and rhombohedral calcite [11]. Calcite is the most abundant polymorph and can be found in numerous sources, such as limestone, eggshells, and some marine shells, such as scallops, oysters, and mussel shells [12–14]. In contrast, the aragonite polymorph is mainly observed in a few organisms, such as cuttlebone, cockle shells, clam shells, and mussel shells [15]. Moreover, the crystal structure of $CaCO_3$ has received much attention because of its industrial and scientific importance [16,17]. Among the three polymorphs, calcite is the most stable polymorph of $CaCO_3$ under ambient conditions, whereas aragonite is metastable and vaterite is the most unstable polymorph [18–20]. In shellfish, both aragonite and calcite are found, depending on the species [21].

Due to its unique physicochemical and structural properties, aragonite $CaCO_3$ is of interest for utilization as a raw material to prepare value-added calcium compounds [10]. Suwannasingha et al. [15] studied the preparation of calcium oxide (CaO) from various calcium sources and reported that aragonite $CaCO_3$ from cuttlebone was completely converted to CaO at 700 dC, while calcite $CaCO_3$ from oyster shells required a temperature of 900 °C to become CaO completely. This finding suggests that the utilization of aragonite $CaCO_3$ as a calcium source is an effective pathway to achieve value-added calcium compounds, such as CaO, with lower energy consumption. CaO is the most effective alkaline metal oxide catalyst for biodiesel production from different oil resources [22]. The reaction time for preparing hydrated calcium lactate ($Ca(CH_3CHOHCOO)_2{\cdot}5H_2O$) from cockle shells, which consist of only aragonite $CaCO_3$, is significantly lower than that from mussel shells and oyster shells, which mainly consist of calcite $CaCO_3$ [10]. Moreover, the production yield of value-added calcium compounds from cockle shells is higher than that obtained from other shells due to the high purity of the calcium sources. Therefore, this research aims to synthesize calcium citrate (CCT) through a mild, simple, and rapid process using citric acid ($C_6H_8O_7$) and aragonite $CaCO_3$, derived from cockle shell waste, as the sustainable calcium source. The effect of $C_6H_8O_7$ concentration on the physicochemical properties of the synthesized CCT was also investigated. The findings observed in this research highlighted the potential of the green synthesis technique with optimization for the productivity of CCT, resulting in a reduction in the production cost for industrial-scale applications. Moreover, waste recycling reduces the greenhouse effect during the production process, which is consistent with the world's carbon neutrality trend and sustainable development goals (SDGs) [23,24].

2. Materials and Methods

2.1. Raw Material Preparation

Cockleshell wastes were used as a renewable calcium source instead of commercial $CaCO_3$ from mining to reduce the use of natural resources and environmental problems from shell waste [10,15]. Cockle shells used in this research were obtained from a coastal landfill in Chonburi Province, Thailand. The collected shells were washed, dried, ground, and sieved through a 100-mesh sieve to obtain aragonite $CaCO_3$ powder [25]. Three different citric acid ($C_6H_8O_7$) concentrations, 2, 3, and 4 M, were prepared by dissolving the desired amount of commercial-grade citric acid powder (99% Fisher Chemical™,UK) in DI water.

2.2. Calcium Citrate (CCT) Preparation

The obtained aragonite $CaCO_3$ powders were converted to calcium citrate (CCT) ($Ca_3(C_6H_5O_7)_2$) in the presence of $C_6H_8O_7$, according to Equation (1) [2]. The effect of $C_6H_8O_7$ concentration (2, 3, and 4 M) on the physicochemical characteristics of the prepared CCT was investigated to optimize the parameters of the synthesis.

$$3CaCO_3(s) + 2C_6H_8O_7(aq) \rightarrow Ca_3(C_6H_5O_7)_2(s) + 3H_2O(l) + 3CO_2(g) \uparrow \quad (1)$$

The preparation process of CCT was carried out by weighing 10 g of powdered $CaCO_3$ and placing it in a glass beaker. Then, 33.30 mL of 2 M citric acid concentration (22.22 mL of 3 M or 16.67 mL of 4 M) was slowly added to each beaker containing powdered $CaCO_3$. The mixture was stirred (300 rpm) until no carbon dioxide (CO_2) evolved, indicating a complete synthesis reaction. After that, the mixture was exposed to atmospheric conditions until it was completely dried, resulting in the formation of white CCT powders. The obtained products were labeled as CCT-2, CCT-3, and CCT-4 for the samples synthesized using 2, 3, and 4 M citric acid solution, respectively. Triplicate experiments were performed for each citric acid solution. Three essential parameters were measured and calculated: reaction time (time for complete synthesis reaction), soluble fraction (the percentage calculated from the mass ratio between the residual CCT mass and the initial mass of CCT used in the test), and percentage yield (the amount ratio between the obtained product (CCT) and utilized precursor (cockle-shell-derived $CaCO_3$).

2.3. Material Characterizations

The functional group in the synthesized CCT sample was analyzed using a Fourier transform infrared (FTIR) spectrophotometer (Spectrum GX, PerkinElmer, Waltham, MA, USA). The spectral profile was recorded in the wavenumber range of 400–4000 cm^{-1} at a resolution of 1 cm^{-1}. The crystal structure and phase purity of the samples were characterized by X-ray diffraction (Bruker AXS, Billerica, MA, USA) using Cu-K_α radiation (λ = 0.15406 nm). The XRD pattern of the sample was analyzed at 2θ angles from 5–60° with an increment of 0.01° at a scan speed of 1 s/step [26]. The obtained diffraction was compared with the Joint Committee on Powder Diffraction Standards (JCPDS) database [27] to clarify the crystalline characteristics and phase purity. The thermal decomposition of the sample was analyzed using thermogravimetric analysis (TG/DTA Pyris Diamond, PerkinElmer, Waltham, MA, USA). The sample (~10 mg) was placed in a calcined alumina crucible without a lid and thermally treated at a constant heating rate of 10 °C/min from room temperature to 900 °C at a constant N_2 gas flow rate of 100 mL/min [28]. The thermally induced mass loss and derivative thermogravimetric characteristics were then interpreted and discussed. The surface morphology and elemental composition of the sample were further characterized by scanning electron microscopy (SEM, VP1450, LEO,

North Billerica, MA, USA). [7] and X-ray fluorescence (XRF, SRS 3400, Bruker, Billerica, MA, USA) [29], respectively. Prior to SEM operation, the sample was coated with gold to increase its conductivity and reduce the charging effect [30]. The solubility of the products was investigated as follows: A typical process involved dissolving 10 g of the CCT sample in 100 mL of DI water, followed by continuous stirring at 100 rpm at room temperature for 1 h. The insoluble fraction(solid) was separated by filtration using a suction pump and dried in an oven (100 °C for 1 h) to determine the weight of the dried solid, which was used to estimate the % solubility. Triplicate experiments were performed for each sample.

3. Results and Discussion

3.1. Functional Groups of CCT

Due to the transmission/absorption of infrared radiation, the Fourier transform infrared (FTIR) technique was utilized to identify the functional groups that existed in the material [31]. Figure 1 shows the FTIR spectra of the CCT products synthesized in this study. Similar spectral patterns across different CCT-2, CCT-3, and CCT-4 samples indicate the presence of the same functional groups in each CCT sample. The FTIR spectra revealed that the functional groups of CCT prepared from the cockle-shell-derived aragonite $CaCO_3$ were consistent with those of CCT products prepared from both $CaCO_3$ [9] and $CaCl_2$ [7] precursors, preliminarily indicating the successful preparation of CCT in this work.

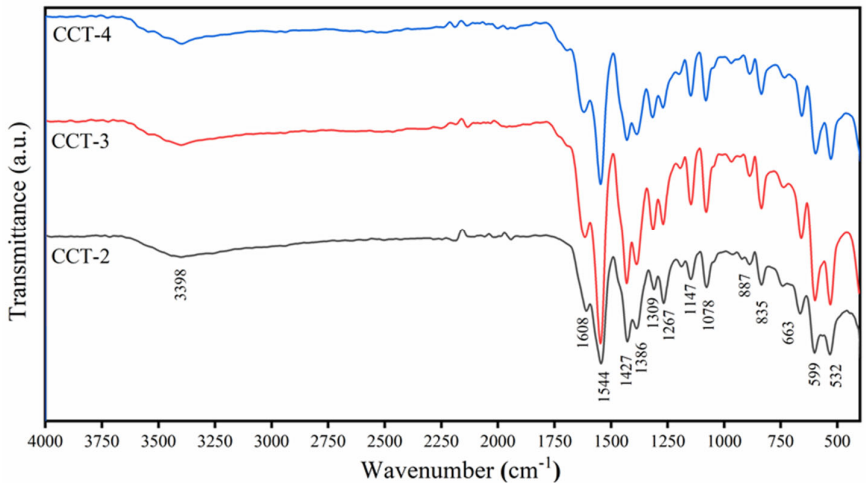

Figure 1. Infrared absorption spectra of calcium citrate derived from aragonite $CaCO_3$ using 2 (CCT2), 3 (CCT3), and 4 (CCT4) M citric acid.

The vibrational modes of the functional groups are described in detail below. The absorption broad band located at 3398 cm^{-1} is attributed to O–H stretching, confirming the presence of H_2O in the CCT crystal structure and/or the moisture absorbed on the sample surface. Two intense absorption peaks observed between 1700 and 1350 cm^{-1} were assigned to the vibrational characteristics of the carboxyl group (–COOH) in all samples. The carboxyl group in CCT can coordinate with Ca^{2+} ions [32]. The characteristic peaks observed at 1608 and 1544 cm^{-1} indicate the presence of the antisymmetric stretching vibration of the carboxylate group ($–COO^–$), while the characteristic peaks observed at 1427 and 1386 cm^{-1} are the symmetric stretching vibrations of $–COO^–$ [7]. The absorption bands at 1309 and 1267 cm^{-1} corresponded to the symmetric C–H bending vibration of the citrate ions ($C_6H_5O_7^{3-}$ or $C_3H_5O(COO)_3^{3-}$). The characteristic peak at 1078 cm^{-1} is assigned to the C–O stretching vibration of $C_3H_5O(COO)_3^{3-}$. The absorption peaks observed at 887 and 835 cm^{-1} are related to the C–C stretching of $C–COO^–$. The peaks at 599 and 532 cm^{-1} corresponded to the out-of-plane O=C–O bending vibration. These

preliminary spectroscopic results suggested that the synthesized product was CCT. However, the exact chemical formula and crystal structure of the product ($Ca_3(C_6H_5O_7)_2$ or $Ca_3(C_6H_5O_7)_2{\cdot}4H_2O$) could not be determined using this characterization technique, and other direct techniques are required to solve this issue.

3.2. Crystal Structure of CCT

X-ray diffraction (XRD) is an effective technique for determining the crystal structure and phase purity of a material [33]. Figure 2 shows the XRD patterns of CCT synthesized from aragonite $CaCO_3$ using 2 (CCT2), 3 (CCT3), and 4 (CCT4) M citric acid. The diffraction patterns of CCT-2, CCT-3, and CCT-4 corresponded well to the standard file of the earlandite mineral [9] or tri-calcium di-citrate tetrahydrate ($Ca_3(C_6H_5O_7)_2{\cdot}4H_2O$) according to ICCD no. 00-069-1272, confirming the successful synthesis of hydrated CCT ($Ca_3(C_6H_5O_7)_2{\cdot}4H_2O$) using aragonite $CaCO_3$. The triclinic crystal structure of $Ca_3(C_6H_5O_7)_2{\cdot}4H_2O$ was reported by Herdtweck et al. [8] with a space group of *P1*. The lattice parameters are a = 5.9466 Å, b = 10.2247 Å, and c = 16.6496 Å. The lattice angles are α = 72.213°, β = 79.718°, and γ = 89.791°. The volume of the unit cell and the number of molecules or formula units (Z) in the unit cell were 947.06 Å^3 and 2, respectively.

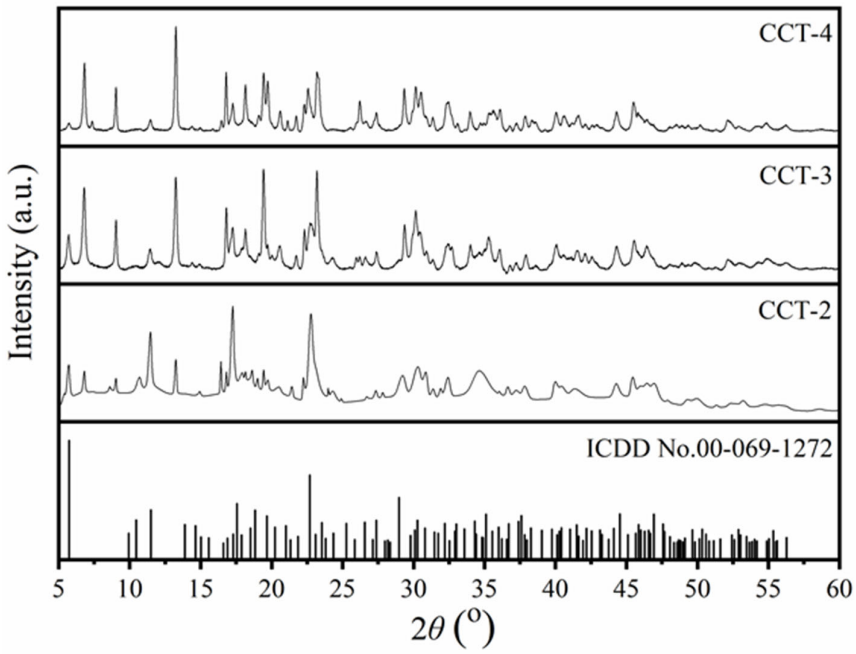

Figure 2. X-ray diffraction patterns of calcium citrate derived from aragonite $CaCO_3$ using 2 (CCT2), 3 (CCT3), and 4 (CCT4) M citric acid compared with the standard ICDD #00-069-1272 of $Ca_3(C_6H_5O_7)_2{\cdot}4H_2O$.

It was also observed that the diffraction peaks of 2θ at 5° and 11° for CCT-3 and CCT-4 samples are relatively lower than that of the CCT-2 sample. These diffraction peaks (2θ at 5° and 11°) corresponded to the (001) and (002) planes of the hydrated form ($Ca_3(C_6H_5O_7)_2{\cdot}4H_2O$). However, higher intensities of the diffraction peaks at 6° and 9° were observed for CCT-3 and CCT-4. Therefore, it could be interpreted that the concentration of citric acid significantly affected the crystal structure of the synthesized CCT. The excess citric acid used in CCT preparation could disturb the formation of CCT, leading to the generation of a side reaction, as shown in Equation (2):

$$Ca_3(C_6H_5O_7)_2\ (CCT) + C_6H_8O_7 \rightarrow 3CaH(C_6H_5O_7) \quad (2)$$

This side reaction causes the deformation of CCT and the formation of calcium hydrogen citrate ($CaH(C_6H_5O_7)$) [2]. Liu et al. [34] also reported that the diffraction peaks at 6° and 9° were identified as the diffraction peaks of anhydrous CCT ($Ca_3(C_6H_5O_7)_2$). Therefore, it could be mentioned that the synthesized CCT product mainly consisted of the tetrahydrated form ($Ca_3(C_6H_5O_7)_2{\cdot}4H_2O$) with the partial anhydrous form ($Ca_3(C_6H_5O_7)_2$). The lowest diffraction intensity at 6° and 9° for CCT-2 indicates the complete precipitation of $Ca_3(C_6H_5O_7)_2{\cdot}4H_2O$, compared to both CCT-3 and CCT-4. The imperfections in the crystal structures of CCT-3 and CCT-4 can be explained by the lower amount of water and the high viscosity of concentrated citric acid in the reaction. In addition, hydrated CCT ($Ca_3(C_6H_5O_7)_2{\cdot}4H_2O$) is more stable than anhydrous CCT, indicating that CCT-2 is consistent with market demand [2].

3.3. Thermal Decomposition of CCT

A thermal analysis experiment was performed to investigate the thermal decomposition behavior [35] of the synthesized CCT, and the resulting thermogravimetric (TG) and derivative thermogravimetric (DTG) profiles were interpreted. Figure 3 shows the thermal decomposition process of the CCT samples measured in the temperature range of 30–900 °C.

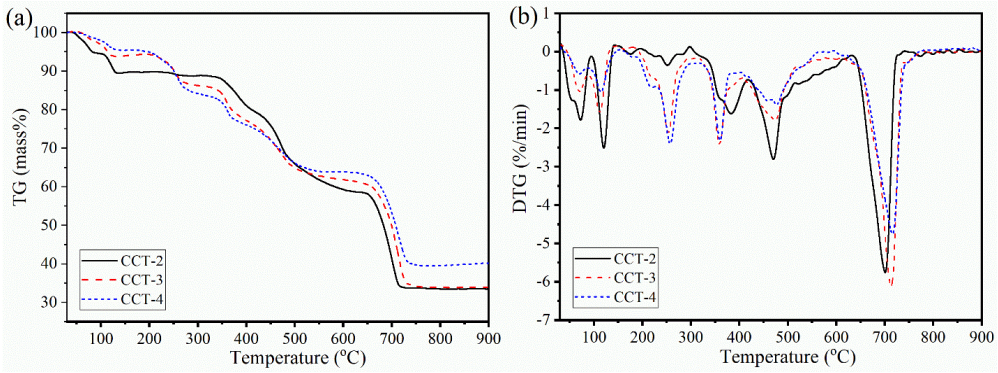

Figure 3. Thermal decomposition behaviors (TG (**a**) and DTG (**b**) curves) of CCT-2, CCT-3, and CCT-4 derived from aragonite $CaCO_3$ using 2, 3, and 4 M citric acid.

Both the TG (Figure 3a) and DTG (Figure 3b) curves of CCT-2 are significantly different from those of CCT-3 and CCT-4. These different thermal decompositions corresponded to the difference in the water content in the crystal structure between CCT-2 and CCT-3 or CCT-4, which is consistent with the difference in the XRD patterns (Figure 2). However, the major decomposition step for all the studied samples revealed similar profiles, as demonstrated by the DTG curves. The thermal decomposition of each sample was divided into four main steps, corresponding to the four different TG mass losses, through the following equations:

First dehydration (30–150 °C):

$$Ca_3(C_6H_5O_7)_2{\cdot}4H_2O(s) \rightarrow Ca_3(C_6H_5O_7)_2{\cdot}2H_2O(s) + 2H_2O(g) \uparrow \quad (3)$$

Second dehydration (150–330 °C):

$$Ca_3(C_6H_5O_7)_2{\cdot}2H_2O(s) \rightarrow Ca_3(C_6H_5O_7)_2(s) + 2H_2O(g) \uparrow \quad (4)$$

Decomposition to $CaCO_3$ (330–600 °C):

$$Ca_3(C_6H_5O_7)_2(s) \rightarrow 3CaCO_3(s) + C_9H_{10}O_5(g) \uparrow \quad (5)$$

Decarbonization (600–730 °C):

$$3CaCO_3(s) \rightarrow 3CaO(s) + 3CO_2(g) \uparrow \quad (6)$$

The mass loss in the first dehydration step (Equation (3)), which appeared in the temperature range from 30 to 150 °C, corresponded to the removal of surface-adsorbed water molecules and a part of the crystal water molecules (water of crystallization) [7]. Two-mole equivalents of water ($2H_2O$) were removed, and the dihydrated product ($Ca_3(C_6H_5O_7)_2 \cdot 2H_2O$) was obtained. The second mass loss (Equation (4), second dehydration step), which occurred at temperatures between 150 and 330 °C, is attributed to the elimination of the remaining constituent water ($2H_2O$). In these first and second dehydration processes, both the adsorbed water on the surface and constituent water ($4H_2O$) were completely removed, and the dehydrated CCT form (anhydrous $Ca_3(C_6H_5O_7)_2$) was obtained [9]. The mass loss of the first and second dehydration processes was evaluated from the TG curve [9,34,35] and was found to be ~10% for the CCT-2 sample, which is slightly lower than the theoretical value of 12.63%. The lower mass loss was related to the presence of absorbed water. However, the mass loss in the first and second dehydrations of CCT-3 and CCT-4 (~4%) was significantly lower than that of CCT-2. The results were consistent with the XRD results, corresponding to the formation of anhydrous $Ca_3(C_6H_5O_7)_2$, resulting in the presence of mixed phases between $Ca_3(C_6H_5O_7)_2 \cdot 4H_2O$ and $Ca_3(C_6H_5O_7)_2$. The mixture of these hydrated and anhydrous crystal forms led to a reduction in the mass loss of both CCT-3 and CCT-4 compared to that of CCT-2.

In addition, the decomposition behavior of the synthesized $Ca_3(C_6H_5O_7)_2 \cdot 4H_2O$ also indicated the environmental difference of the constituent water ($4H_2O$) in the crystal structure. According to the dehydration process, $2H_2O$ was first thermally eliminated from tetra-hydrated CCT ($Ca_3(C_6H_5O_7)_2 \cdot 4H_2O$), followed by the removal of the remaining two molecules of H_2O from $Ca_3(C_6H_5O_7)_2 \cdot 2H_2O$, forming anhydrous $Ca_3(C_6H_5O_7)_2$. Therefore, the exact chemical formula of hydrated calcium citrate can be rewritten as $[Ca_3(C_6H_5O_7)_2(H_2O)_2] \cdot 2H_2O$, which is consistent with the findings in the literature [7,8]. This could also be interpreted as the inner water, or $(H_2O)_2$ in the $[Ca_3(C_6H_5O_7)_2(H_2O)_2] \cdot 2H_2O$, chemically interacting with $Ca_3(C_6H_5O_7)_2$ with a stronger interaction than the outer water, or $2H_2O$. In this case, the outer water was first thermally removed, followed by the removal of the inner water, which is consistent with the TG/DTG profile of CCT, especially CCT-2.

A TG mass loss of ~34% in the third step (decomposition to $CaCO_3$) with three DTG peaks was observed at the temperature from 330 to 600 °C. This thermal step was assigned to the thermal decomposition of anhydrous $Ca_3(C_6H_5O_7)_2$, associated with the formation of $CaCO_3$ (Equation (5)) [7,9]. In this thermal decomposition step, syringic acid ($C_9H_{10}O_5$) [36,37] was eliminated as CO, CO_2, and H_2O [7,8]. The final thermal decomposition step with a mass loss of ~25% appeared in the temperature range from 630 to 730 °C. This step is related to the decomposition of $CaCO_3$ with the elimination of CO_2 (decarbonization), as expressed in Equation (6), resulting in the formation of CaO as the final decomposition product. The TG mass loss in the third and final steps was also close to the theoretical values of 34.74% and 23.16%, respectively. The thermal decomposition characteristics of all $Ca_3(C_6H_5O_7)_2 \cdot 4H_2O$ samples prepared from cockle-shell-derived aragonite $CaCO_3$ in this work were similar to those of $Ca_3(C_6H_5O_7)_2 \cdot 4H_2O$ prepared from oyster-shell-derived calcite $CaCO_3$ [15]. However, the complete thermal temperature of the sample obtained in this work was found to be ~730 °C, which is slightly lower than that of the sample prepared from calcite (900 °C) [15].

3.4. Purities of CCT Determined by XRF

X-ray fluorescence (XRF), a non-destructive testing technique, was used to evaluate the elemental composition of the solid-state sample (CCT) synthesized in this work [38]. A secondary fluorescent emission profile was observed owing to the excitation of atomic inner-shell electrons by the primary X-ray beam [39]. Table 1 lists the chemical compositions of the synthesized CCT samples determined using the XRF technique. The results showed that all synthesized CCT-2, CCT-3, and CCT-4 samples mainly consisted of CaO with the same wt% value (main composition, 98.2 wt%). However, other metal oxides were also observed at approximate amounts in all samples (minor compositions, 1.8 wt%).

Table 1. Elemental compositions of CCT-2, CCT-3, and CCT-4 were analyzed by X-ray fluorescence (XRF) technique.

Elemental Compositions		Elemental Contents/wt%		
		CCT-2	**CCT-3**	**CCT-4**
Major composition				
Calcium oxide	CaO	98.1778	98.1805	98.1857
Minor compositions				
Sodium oxide	Na_2O	0.8520	0.8200	0.8410
Magnesium oxide	MgO	0.0462	0.0414	0.0470
Aluminum oxide	Al_2O_3	0.0323	0.0331	0.0431
Silicon dioxide	SiO_2	0.0854	0.0903	0.0925
Phosphorus pentoxide	P_2O_5	0.0193	0.0187	0.0209
Sulfur trioxide	SO_3	0.1370	0.1330	0.1430
Chlorine	Cl	0.0212	0.0192	0.0211
Potassium oxide	K_2O	0.0123	0.0097	0.0126
Cobalt oxide	Co_2O_3	-	0.0211	-
Zinc oxide	ZnO	-	0.0146	-
Strontium oxide	SrO	0.4350	0.4450	0.455
Ferrous oxide	Fe_2O_3	0.1470	0.1450	0.1460
Summations		~100	~100	~100

The experimental results observed in this work highlighted that cockle shell waste is an alternative renewable calcium source for preparing high-purity CCT without toxic elements, such as cadmium (Cd), arsenic (As), mercury (Hg), and lead (Pb). High-quality CCT products prepared from cockle shells (aragonite $CaCO_3$) have attracted increasing attention in the food industry as both calcium supplements and food additives [2]. The synthesized CCT product could also be applied for bone reparation [25] due to its faster absorbability than calcium phosphate [40] and hydroxyapatite [41].

3.5. Morphologies of CCT

The scanning electron microscope (SEM), a type of electron microscope, generates the sample surface images using a focused electron beam, which reveals the morphological characteristics of the imaged sample [42]. Figure 4 illustrates the morphologies of the CCT samples synthesized from aragonite $CaCO_3$ in the presence of different citric acid concentrations. Morphological analysis revealed that the CCT synthesized from aragonite crystals presented irregular plate-like crystallites that aggregated into enlarged irregular

particles. The dimensions of the particles are in the range of 0.3–2 µm. The SEM images of CCT-2, CCT-3, and CCT-4, synthesized from the aragonite $CaCO_3$ precursor, presented morphological characteristics similar to those of the earlandite ($Ca_3(C_6H_5O_7)_2{\cdot}4H_2O$) synthesized from the calcite $CaCO_3$ precursor [9], indicating the successful preparation of $Ca_3(C_6H_5O_7)_2{\cdot}4H_2O$.

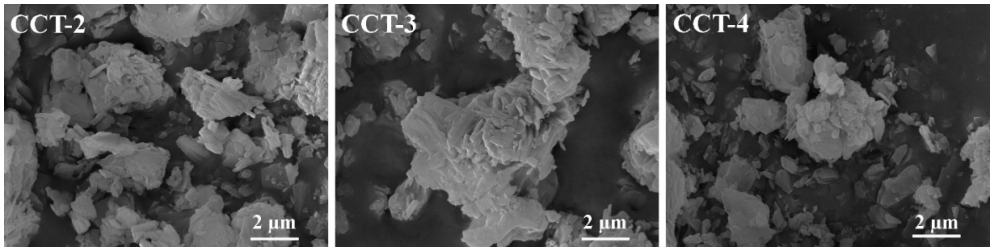

Figure 4. SEM images at a magnification of 20k× of CCT particles derived from aragonite $CaCO_3$ using 2, 3, and 4 M citric acid.

3.6. Preparation Results

Equation (1) represents the preparation of CCT ($Ca_3(C_6H_5O_7)_2$), which was obtained through reactive crystallization [2]. During the reaction, as shown in the equation, $3Ca^{2+}$ and $2C_6H_5O_7{}^{3-}$ ions were solvated by water with the elimination of CO_2. After that, the solvent (water) could evaporate from the reaction, causing the crystallization process in a supersaturation situation. The saturated point induced the formation of a $3Ca^{2+}$-$2C_6H_5O_7{}^{3-}$ nucleus, followed by the $Ca_3(C_6H_5O_7)_2$ crystal growth process. However, the hydrated form of the product was also fabricated due to the presence of an aqueous-based citric acid solution, resulting in the formation of $Ca_3(C_6H_5O_7)_2{\cdot}4H_2O$ or $[Ca_3(C_6H_5O_7)_2(H_2O)_2]{\cdot}2H_2O$. Consequently, $Ca_3(C_6H_5O_7)_2{\cdot}4H_2O$ was obtained in this work using a cockle-shell-derived aragonite $CaCO_3$ precursor, and the effect of citric acid concentration (2, 3, and 4 M) on the physicochemical properties of the products was investigated using FTIR, XRD, TG/DTG, and SEM.

In addition, after applying the same preparation conditions, the parameters investigated, including the production yield, reaction time, and soluble fraction of all prepared CCT samples, were obtained, and the results are reported in Table 2.

Table 2. The production parameters of CCT-2, CCT-3, and CCT-4 from aragonite $CaCO_3$.

Samples	Reaction Time (min)	Production Yields (%)	Soluble Fractions (%)
CCT-2	54	98.57 ± 1.46	92.51 ± 1.24
CCT-3	67	93.14 ± 1.37	88.72 ± 1.33
CCT-4	85	88.63 ± 1.42	84.17 ± 1.29

It was found that the reaction time increased with increasing citric acid concentration due to the higher amount of citrate ions ($C_6H_5O_7{}^{3-}$), which increased the viscosity of the synthesis reaction. However, at high citric acid concentrations, the reaction formed CCT precipitation with a rigid structure, causing a low soluble fraction percentage. The production yields were calculated to be 98.57%, 93.14%, and 88.63% when 2, 3, and 4 M citric acid solutions were used in the production reaction, respectively. The lowest yield obtained from the highest citric acid concentration was consistent with the longer reaction time (85 min). The high viscosity and density of citric acid [43] compared to water inhibited the production progress of the CCT product, resulting in a decreased production yield.

It was also observed that an increase in citric acid concentration caused the formation of a higher proportion of anhydrous CCT ($Ca_3(C_6H_5O_7)_2$) in the mixed precipitate products ($Ca_3(C_6H_5O_7)_2{\cdot}4H_2O$ + $Ca_3(C_6H_5O_7)_2$). The increased proportion of anhydrous $Ca_3(C_6H_5O_7)_2$ was verified and discussed in the XRD and TG/DTG results. The results suggest that the concentration of citric acid is the key factor [44] that significantly impacts the CCT crystal forms (hydrated or anhydrous product) and their physicochemical properties, as well as the production yield, reaction time, and soluble fraction of CCT. From the results obtained, it can be concluded that 2 M citric acid is the optimum condition for preparing hydrated calcium citrate ($Ca_3(C_6H_5O_7)_2{\cdot}4H_2O$) with the highest yield percentage, lowest reaction time, and highest soluble fraction. The CCT products in this work were obtained with a short time consumption (<85 min), high yield, and high purity of the product, and the differences in some properties from calcium citrate (earlandite) synthesis using microorganisms [7–9]. This makes the product obtained by this method low-cost compared with those obtained using other synthesis methods [7–9]. Furthermore, the obtained hydrated CCT is considered to be the CCT form that meets the market demand for application as a calcium supplement and food additive [2], and for bone reparation [25].

4. Conclusions

With the addition of citric acid ($C_6H_8O_7$), calcium citrate (CCT, $Ca_3(C_6H_5O_7)_2$) was successfully synthesized using aragonite $CaCO_3$, derived from cockle shell waste as a green calcium source. Three different $C_6H_8O_7$ concentrations (2, 3, and 4 M) were used in the synthesis, and CCT-2, CCT-3, and CCT-4 products were obtained, respectively. The vibrational spectroscopy of all CCT, revealed by FTIR spectra, shows the same functional groups corresponding to the citrate anion. However, the XRD patterns and thermal decomposition (TG/DTG) profiles revealed differences in the number of constituent water molecules in the $Ca_3(C_6H_5O_7)_2$ crystal structure. Using 2 M citric acid, $Ca_3(C_6H_5O_7)_2{\cdot}4H_2O$ or $[Ca_3(C_6H_5O_7)_2(H_2O)_2]{\cdot}2H_2O$ was obtained for CCT-2, whereas an anhydrous $Ca_3(C_6H_5O_7)_2$ phase was further observed by using 3 and 4 M citric acid, thereby obtaining the mixture between $[Ca_3(C_6H_5O_7)_2(H_2O)_2]{\cdot}2H_2O$ and $Ca_3(C_6H_5O_7)_2$. The mass loss of the first and second dehydrations of CCT-3 and CCT-4 were significantly lower than those of CCT-2. These findings are consistent with the XRD results. However, the constituent water did not alter the morphological characteristics of the as-prepared CCT products. The XRF results revealed the high purity of the CCT products, which could be further considered as food supplements and bone reparations. Based on the production yield, reaction time, and soluble fraction percentage, the optimum concentration of citric acid was determined to be 2 M. All results highlighted that aragonite $CaCO_3$ derived from cockle shell waste could be effectively utilized as a renewable calcium source, instead of limited and non-renewable calcium ores, to synthesize CCT product. This has led to the development of green and sustainable techniques to reduce natural resource use and shell waste, which have environmental implications.

Author Contributions: Conceptualization, B.B. and N.L.; methodology, P.C. and C.S.; investigations, P.C. and C.S.; data curation, W.B. and N.L.; writing—original draft preparation, W.B. and S.S; writing—review and editing, P.R. and B.B.; visualization, W.B.; supervision, S.S. and W.B.; project administration, B.B.; funding acquisition, P.R. All authors have read and agreed to the published version of the manuscript.

Funding: This work is a result of the project entitled "Conversion of shell/eggshell biowastes for sustainable environmental remediation" Grant No. RE-KRIS/FF67/030 by King Mongkut's Institute of Technology Ladkrabang (KMITL), which received funding support from the NSRE.

Data Availability Statement: Data are contained within the article.

Acknowledgments: The authors would like to thank the Scientific Instruments Center KMITL for supporting TGA, FTIR, XRD, and SEM techniques.

Conflicts of Interest: The authors declare that they have no known competing financial interests or personal relationships that could have appeared to influence the work reported in this paper.

References

1. Hany, M.; Wuyts, S.; Abouelnasr, A.A.; Zidan, A.; Demerdash, H.M.; Hussein, H.A.S.M.; Arida, R.E.; Elsharkawi, S.M.; Kramers, C.; Torensma, B. Comparison of calcium citrate and calcium carbonate absorption in patients with a Roux-en-Y gastric bypass, sleeve gastrectomy, and one-anastomosis gastric bypass: A double-blind, randomized cross-over trial. *Surg. Obes. Relat. Dis.* **2025**, *21*, 471–481. [CrossRef] [PubMed]
2. Yan, H.; Liu, Y.; Peng, H.; Li, K.; Li, C.; Jiang, S.; Chen, M.; Han, D.; Gong, J. Improving calcium citrate food functions through spherulitic growth in reactive crystallization and a mechanism study. *Food Chem.* **2023**, *404*, 134550. [CrossRef]
3. Tondapu, P.; Provost, D.; Adams-Huet, B.; Sims, T.; Chang, C.; Sakhaee, K. Comparison of the absorption of calcium carbonate and calcium citrate after Roux-en-Y gastric bypass. *Obes. Surg.* **2009**, *19*, 1256–1261. [CrossRef]
4. Wang, L.-m.; Wang, W.; Li, X.-C.; Peng, L.; Lin, Z.-Q. Calcium citrate: A new biomaterial that can enhance bone formation in situ. *Chin. J. Traumatol.* **2012**, *15*, 291–296.
5. Kaduk, J.A. Crystal structure of aqua (citric acid)(hydrogen citrato) calcium monohydrate, $[Ca(HC_6H_5O_7)(H_3C_6H_5O_7)(H_2O)]\cdot H_2O$, from synchrotron X-ray powder data, and DFT-optimized crystal structure of existing calcium hydrogen citrate trihydrate, $[Ca(HC_6H_5O_7)(H_2O)_3]$. *Struct. Rep.* **2020**, *76*, 1689–1693. [CrossRef]
6. Kaduk, J.A. Crystal structures of tricalcium citrates. *Powder Diffr.* **2018**, *33*, 98–107. [CrossRef]
7. Li, J.; Liu, Y.; Gao, Y.; Zhong, L.; Zou, Q.; Lai, X. Preparation and properties of calcium citrate nanosheets for bone graft substitute. *Bioengineered* **2016**, *7*, 376–381. [CrossRef] [PubMed]
8. Herdtweck, E.; Kornprobst, T.; Sieber, R.; Straver, L.; Plank, J. Crystal structure, synthesis, and properties of tri-calcium di-citrate tetra-hydrate $[Ca_3(C_6H_5O_7)_2(H_2O)_2]\cdot 2H_2O$. *Z. Anorg. Allg. Chem.* **2011**, *637*, 655–659. [CrossRef]
9. Wei, S.; Sun, M. Transformation of calcite ($CaCO_3$) into earlandite $[Ca_3(C_6H_5O_7)_2\cdot 4H_2O]$ by the fungus Trichoderma asperellum BDH65. *Int. Biodeterior. Biodegrad.* **2021**, *163*, 105278. [CrossRef]
10. Seesanong, S.; Seangarun, C.; Boonchom, B.; Phutphat, S.; Rungrojchaipon, P.; Montri, N.; Thompho, S.; Boonmee, W.; Laohavisuti, N. Efficient, green, and low-cost conversion of bivalve-shell wastes to value-added calcium lactate. *ACS Omega* **2023**, *8*, 27044–27055. [CrossRef]
11. Sand, K.; Rodriguez-Blanco, J.; Makovicky, E.; Benning, L.G.; Stipp, S. Crystallization of $CaCO_3$ in water–alcohol mixtures: Spherulitic growth, polymorph stabilization, and morphology change. *Cryst. Growth Des.* **2012**, *12*, 842–853. [CrossRef]
12. Cubillas, P.; Köhler, S.; Prieto, M.; Chaïrat, C.; Oelkers, E.H. Experimental determination of the dissolution rates of calcite, aragonite, and bivalves. *Chem. Geol.* **2005**, *216*, 59–77. [CrossRef]
13. Pan, L.; Li, Q.; Zhou, Y.; Song, N.; Yu, L.; Wang, X.; Xiong, K.; Yap, L.; Huo, J. Effects of different calcium sources on the mineralization and sand curing of $CaCO_3$ by carbonic anhydrase-producing bacteria. *RSC Adv.* **2019**, *9*, 40827–40834. [CrossRef]
14. Sasaki, K.; Yamashita, T.; Tsunekawa, M. Synthesis of Aragonite from Calcined Scallop Shells at Ambient Temperatures and Their Morphological Characterization by FE-SEM. *Shigen-to-Sozai* **2002**, *118*, 553–558. [CrossRef]
15. Suwannasingha, N.; Kantavong, A.; Tunkijjanukij, S.; Aenglong, C.; Liu, H.-B.; Klaypradit, W. Effect of calcination temperature on structure and characteristics of calcium oxide powder derived from marine shell waste. *J. Saudi Chem. Soc.* **2022**, *26*, 101441. [CrossRef]
16. Cölfen, H. Precipitation of carbonates: Recent progress in controlled production of complex shapes. *Curr. Opin. Colloid Interface Sci.* **2003**, *8*, 23–31. [CrossRef]
17. Ramakrishna, C.; Thenepalli, T.; Han, C.; Ahn, J.-W. Synthesis of aragonite-precipitated calcium carbonate from oyster shell waste via a carbonation process and its applications. *Korean J. Chem. Eng.* **2017**, *34*, 225–230. [CrossRef]
18. Gopi, S.; Subramanian, V.; Palanisamy, K. Aragonite–calcite–vaterite: A temperature influenced sequential polymorphic transformation of $CaCO_3$ in the presence of DTPA. *Mater. Res. Bull.* **2013**, *48*, 1906–1912. [CrossRef]
19. Jimoh, O.A.; Ariffin, K.S.; Hussin, H.B.; Temitope, A.E. Synthesis of precipitated calcium carbonate: A review. *Carbonates Evaporites* **2018**, *33*, 331–346. [CrossRef]
20. Kirboga, S.; Oner, M. Effect of the experimental parameters on calcium carbonate precipitation. *Chem. Eng. J.* **2013**, *32*, 2119–2124.
21. Zaitsev, A.V.; Astapov, I.A. Study of the Composition and Properties of Bivalve Mollusk Shells as Promising Bio-Indifferent Materials for Photocatalytic Applications (Example of Practical Use). *Catalysts* **2023**, *14*, 16. [CrossRef]
22. Basumatary, S.F.; Brahma, S.; Hoque, M.; Das, B.K.; Selvaraj, M.; Brahma, S.; Basumatary, S. Advances in CaO-based catalysts for sustainable biodiesel synthesis. *Green Energy Resour.* **2023**, *1*, 100032. [CrossRef]

23. Boey, P.-l.; Maniam, G.P.; Abd Hamid, S.; Ali, D.M.H. Utilization of waste cockle shell (*Anadara granosa*) in biodiesel production from palm olein: Optimization using response surface methodology. *Fuel* **2011**, *90*, 2353–2358. [CrossRef]
24. Ruslan, H.N.; Muthusamy, K.; Jaafar, M.; Zamri, N.A.; Jaya, R.P. Mechanical properties of mortar with Anadara Granosa waste as partial sand replacement. *Open Civ. Eng. J.* **2023**, *17*, e187414952303280. [CrossRef]
25. Mahmood, S.K.; Zakaria, M.Z.A.B.; Razak, I.S.B.A.; Yusof, L.M.; Jaji, A.Z.; Tijani, I.; Hammadi, N.I. Preparation and characterization of cockle shell aragonite nanocomposite porous 3D scaffolds for bone repair. *Biochem. Biophys. Rep.* **2017**, *10*, 237–251. [CrossRef] [PubMed]
26. Seesanong, S.; Wongchompoo, Y.; Boonchom, B.; Sronsri, C.; Laohavisuti, N.; Chaiseeda, K.; Boonmee, W. Economical and environmentally friendly track of biowaste recycling of scallop shells to calcium lactate. *ACS Omega* **2022**, *7*, 14756–14764. [CrossRef] [PubMed]
27. Wong-Ng, W.; McMurdie, H.; Hubbard, C.; Mighell, A.D. JCPDS-ICDD research associateship (cooperative program with NBS/NIST). *J. Res. Natl. Inst. Stand. Technol.* **2001**, *106*, 1013. [CrossRef]
28. Sronsri, C.; Boonchom, B. Thermal kinetic analysis of a complex process from a solid-state reaction by deconvolution procedure from a new calculation method and related thermodynamic functions of $Mn_{0.90}Co_{0.05}Mg_{0.05}HPO_4{\cdot}3H_2O$. *Trans. Nonferrous Met. Soc. China* **2018**, *28*, 1887–1902. [CrossRef]
29. Khan, M.M. X-ray fluorescence spectroscopy. In *Photocatalysts: Synthesis and Characterization Methods*; Elsevier: Amsterdam, The Netherlands, 2025; pp. 225–237.
30. Yuan, J.; Yang, L.; Yu, P.; Tang, N.; Liu, L.; Wang, W.; Wang, P.; Yang, Q.; Guo, S.; Li, J. Comparison and development of scanning electron microscope techniques for delicate plant tissues. *Plant Sci.* **2024**, *340*, 111963. [CrossRef]
31. Gong, Y.; Chen, X.; Wu, W. Application of fourier transform infrared (FTIR) spectroscopy in sample preparation: Material characterization and mechanism investigation. *Adv. Sample Prep.* **2024**, *11*, 100122. [CrossRef]
32. Ding, X.-M.; Peng, L.; Wen, F.; Tan, Z.-W.; Mu, Z.-L. Simulated body fluid immersion method for assessing biological characteristics of calcium citrate. *Chin. J. Tissue Eng. Res.* **2013**, *17*, 6811.
33. Ali, A.; Chiang, Y.W.; Santos, R.M. X-ray diffraction techniques for mineral characterization: A review for engineers of the fundamentals, applications, and research directions. *Minerals* **2022**, *12*, 205. [CrossRef]
34. Liu, X.-C.; Kirkensgaard, J.J.; Skibsted, L.H. Hydrates of calcium citrate and their interconversion in relation to calcium bioaccessibility. *Food Res. Int.* **2021**, *140*, 109867. [CrossRef]
35. El-Sayed, S.A.; Khass, T.M.; Mostafa, M.E. Thermal degradation behaviour and chemical kinetic characteristics of biomass pyrolysis using TG/DTG/DTA techniques. *Biomass Convers. Biorefinery* **2024**, *14*, 17779–17803. [CrossRef]
36. Mirza, A.C.; Panchal, S.S.; Allam, A.A.; Othman, S.I.; Satia, M.; Mandhane, S.N. Syringic acid ameliorates cardiac, hepatic, renal and neuronal damage induced by chronic hyperglycaemia in Wistar rats: A behavioural, biochemical and histological analysis. *Molecules* **2022**, *27*, 6722. [CrossRef]
37. Srinivasulu, C.; Ramgopal, M.; Ramanjaneyulu, G.; Anuradha, C.; Kumar, C.S. Syringic acid (SA)—A review of its occurrence, biosynthesis, pharmacological and industrial importance. *Biomed. Pharmacother.* **2018**, *108*, 547–557. [CrossRef]
38. Cahill, J.; Davis, V.; King, C.; Miller, L.; Norrgard, T.; Castano, C.E.; Mohammadi, R.; Rojas, J.; Goddard, B. Modeling and benchmarking XRF analysis using MCNP for applications in accident tolerant fuel and cladding. *Prog. Nucl. Energy* **2025**, *178*, 105487. [CrossRef]
39. Janssens, K. X-Ray Fluorescence Analysis. In *Handbook of Spectroscopy: Second, Enlarged Edition*; John Wiley & Sons: Hoboken, NJ, USA, 2014; pp. 449–506.
40. Richter, R.F.; Vater, C.; Korn, M.; Ahlfeld, T.; Rauner, M.; Pradel, W.; Stadlinger, B.; Gelinsky, M.; Lode, A.; Korn, P. Treatment of critical bone defects using calcium phosphate cement and mesoporous bioactive glass providing spatiotemporal drug delivery. *Bioact. Mater.* **2023**, *28*, 402–419. [CrossRef]
41. Ielo, I.; Calabrese, G.; De Luca, G.; Conoci, S. Recent advances in hydroxyapatite-based biocomposites for bone tissue regeneration in orthopedics. *Int. J. Mol. Sci.* **2022**, *23*, 9721. [CrossRef]
42. Khan, M.M. Scanning electron microscopy. In *Photocatalysts: Synthesis and Characterization Methods*; Elsevier: Amsterdam, The Netherlands, 2025; pp. 281–294.
43. Moreno, J.; Peinado, R. *Enological Chemistry*; Academic Press: Cambridge, MA, USA, 2012.
44. Olatide, M.; Oladele, E.; Lajide, L.; Oluwasina, O. The effect of citric acid concentration, reaction temperature and time on the esterification of some varieties of yam flour in Nigeria. *Discov. Chem.* **2024**, *1*, 69. [CrossRef]

Disclaimer/Publisher's Note: The statements, opinions and data contained in all publications are solely those of the individual author(s) and contributor(s) and not of MDPI and/or the editor(s). MDPI and/or the editor(s) disclaim responsibility for any injury to people or property resulting from any ideas, methods, instructions or products referred to in the content.